Article

Direct photon cross section with conversions at CDF

CDF Collaboration

CLARK, Allan Geoffrey (Collab.), D'ONOFRIO, Monica (Collab.), WU, Xin (Collab.)

Abstract

We present a measurement of the isolated direct photon cross section in $p\bar{p}$ collisions at $\sqrt{s}$=1.8 TeV and |η|

Reference

CDF Collaboration, CLARK, Allan Geoffrey (Collab.), D'ONOFRIO, Monica (Collab.), WU, Xin (Collab.). Direct photon cross section with conversions at CDF. *Physical Review. D*, 2004, vol. 70, no. 07, p. 074008

DOI : 10.1103/PhysRevD.70.074008

Direct photon cross section with conversions at CDF

D. Acosta,[14] T. Affolder,[7] M. G. Albrow,[13] D. Ambrose,[36] D. Amidei,[27] K. Anikeev,[26] J. Antos,[1] G. Apollinari,[13] T. Arisawa,[50] A. Artikov,[11] W. Ashmanskas,[2] F. Azfar,[34] P. Azzi-Bacchetta,[35] N. Bacchetta,[35] H. Bachacou,[24] W. Badgett,[13] A. Barbaro-Galtieri,[24] V. E. Barnes,[39] B. A. Barnett,[21] S. Baroiant,[5] M. Barone,[15] G. Bauer,[26] F. Bedeschi,[37] S. Behari,[21] S. Belforte,[47] W. H. Bell,[17] G. Bellettini,[37] J. Bellinger,[51] D. Benjamin,[12] A. Beretvas,[13] A. Bhatti,[41] M. Binkley,[13] D. Bisello,[35] M. Bishai,[13] R. E. Blair,[2] C. Blocker,[4] K. Bloom,[27] B. Blumenfeld,[21] A. Bocci,[41] A. Bodek,[40] G. Bolla,[39] A. Bolshov,[26] D. Bortoletto,[39] J. Boudreau,[38] C. Bromberg,[28] E. Brubaker,[24] J. Budagov,[11] H. S. Budd,[40] K. Burkett,[13] G. Busetto,[35] K. L. Byrum,[2] S. Cabrera,[12] M. Campbell,[27] W. Carithers,[24] D. Carlsmith,[51] A. Castro,[3] D. Cauz,[47] A. Cerri,[24] L. Cerrito,[20] J. Chapman,[27] C. Chen,[36] Y. C. Chen,[1] M. Chertok,[5] G. Chiarelli,[37] G. Chlachidze,[13] F. Chlebana,[13] M. L. Chu,[1] J. Y. Chung,[32] W.-H. Chung,[51] Y. S. Chung,[40] C. I. Ciobanu,[20] A. G. Clark,[16] M. Coca,[40] A. Connolly,[24] M. Convery,[41] J. Conway,[43] M. Cordelli,[15] J. Cranshaw,[45] R. Culbertson,[13] D. Dagenhart,[4] S. D'Auria,[17] P. de Barbaro,[40] S. De Cecco,[42] S. Dell'Agnello,[15] M. Dell'Orso,[37] S. Demers,[40] L. Demortier,[41] M. Deninno,[3] D. De Pedis,[42] P. F. Derwent,[13] C. Dionisi,[42] J. R. Dittmann,[13] A. Dominguez,[24] S. Donati,[37] M. D'Onofrio,[16] T. Dorigo,[35] N. Eddy,[20] R. Erbacher,[13] D. Errede,[20] S. Errede,[20] R. Eusebi,[40] S. Farrington,[17] R. G. Feild,[52] J. P. Fernandez,[39] C. Ferretti,[27] R. D. Field,[14] I. Fiori,[37] B. Flaugher,[13] L. R. Flores-Castillo,[38] G. W. Foster,[13] M. Franklin,[18] J. Friedman,[26] I. Furic,[26] M. Gallinaro,[41] M. Garcia-Sciveres,[24] A. F. Garfinkel,[39] C. Gay,[52] D. W. Gerdes,[27] E. Gerstein,[9] S. Giagu,[42] P. Giannetti,[37] K. Giolo,[39] M. Giordani,[47] P. Giromini,[15] V. Glagolev,[11] D. Glenzinski,[13] M. Gold,[30] N. Goldschmidt,[27] J. Goldstein,[34] G. Gomez,[8] M. Goncharov,[44] I. Gorelov,[30] A. T. Goshaw,[12] Y. Gotra,[38] K. Goulianos,[41] A. Gresele,[3] C. Grosso-Pilcher,[10] M. Guenther,[39] J. Guimaraes da Costa,[18] C. Haber,[24] S. R. Hahn,[13] E. Halkiadakis,[40] C. Hall,[18] R. Handler,[51] F. Happacher,[15] K. Hara,[48] R. M. Harris,[13] F. Hartmann,[22] K. Hatakeyama,[41] J. Hauser,[6] J. Heinrich,[36] M. Hennecke,[22] M. Herndon,[21] C. Hill,[7] A. Hocker,[40] K. D. Hoffman,[10] S. Hou,[1] B. T. Huffman,[34] R. Hughes,[32] J. Huston,[28] C. Issever,[7] J. Incandela,[7] G. Introzzi,[37] M. Iori,[42] A. Ivanov,[40] Y. Iwata,[19] B. Iyutin,[26] E. James,[13] M. Jones,[39] T. Kamon,[44] J. Kang,[27] M. Karagoz Unel,[31] S. Kartal,[13] H. Kasha,[52] Y. Kato,[33] R. D. Kennedy,[13] R. Kephart,[13] B. Kilminster,[40] D. H. Kim,[23] H. S. Kim,[20] M. J. Kim,[9] S. B. Kim,[23] S. H. Kim,[48] T. H. Kim,[26] Y. K. Kim,[10] M. Kirby,[12] L. Kirsch,[4] S. Klimenko,[14] P. Koehn,[32] K. Kondo,[50] J. Konigsberg,[14] A. Korn,[26] A. Korytov,[14] J. Kroll,[36] M. Kruse,[12] V. Krutelyov,[44] S. E. Kuhlmann,[2] N. Kuznetsova,[13] A. T. Laasanen,[39] S. Lami,[41] S. Lammel,[13] J. Lancaster,[12] K. Lannon,[32] M. Lancaster,[25] R. Lander,[5] A. Lath,[43] G. Latino,[30] T. LeCompte,[2] Y. Le,[21] J. Lee,[40] S. W. Lee,[44] N. Leonardo,[26] S. Leone,[37] J. D. Lewis,[13] K. Li,[52] C. S. Lin,[13] M. Lindgren,[6] T. M. Liss,[20] T. Liu,[13] D. O. Litvintsev,[13] N. S. Lockyer,[36] A. Loginov,[29] M. Loreti,[35] D. Lucchesi,[35] P. Lukens,[13] L. Lyons,[34] J. Lys,[24] R. Madrak,[18] K. Maeshima,[13] P. Maksimovic,[21] L. Malferrari,[3] M. Mangano,[37] G. Manca,[34] M. Mariotti,[35] M. Martin,[21] A. Martin,[52] V. Martin,[31] M. Martínez,[13] P. Mazzanti,[3] K. S. McFarland,[40] P. McIntyre,[44] M. Menguzzato,[35] A. Menzione,[37] P. Merkel,[13] C. Mesropian,[41] A. Meyer,[13] T. Miao,[13] R. Miller,[28] J. S. Miller,[27] S. Miscetti,[15] G. Mitselmakher,[14] N. Moggi,[3] R. Moore,[13] T. Moulik,[39] M. Mulhearn,[26] A. Mukherjee,[13] T. Muller,[22] A. Munar,[36] P. Murat,[13] J. Nachtman,[13] S. Nahn,[52] I. Nakano,[19] R. Napora,[21] F. Niell,[27] C. Nelson,[13] T. Nelson,[13] C. Neu,[32] M. S. Neubauer,[26] C. Newman-Holmes,[13] T. Nigmanov,[38] L. Nodulman,[2] S. H. Oh,[12] Y. D. Oh,[23] T. Ohsugi,[19] T. Okusawa,[33] W. Orejudos,[24] C. Pagliarone,[37] F. Palmonari,[37] R. Paoletti,[37] V. Papadimitriou,[45] J. Patrick,[13] G. Pauletta,[47] M. Paulini,[9] T. Pauly,[34] C. Paus,[26] D. Pellett,[5] A. Penzo,[47] T. J. Phillips,[12] G. Piacentino,[37] J. Piedra,[8] K. T. Pitts,[20] A. Pompoš,[39] L. Pondrom,[51] G. Pope,[38] T. Pratt,[34] F. Prokoshin,[11] J. Proudfoot,[2] F. Ptohos,[15] O. Poukhov,[11] G. Punzi,[37] J. Rademacker,[34] A. Rakitine,[26] F. Ratnikov,[43] H. Ray,[27] A. Reichold,[34] P. Renton,[34] M. Rescigno,[42] F. Rimondi,[3] L. Ristori,[37] W. J. Robertson,[12] T. Rodrigo,[8] S. Rolli,[49] L. Rosenson,[26] R. Roser,[13] R. Rossin,[35] C. Rott,[39] A. Roy,[39] A. Ruiz,[8] D. Ryan,[49] A. Safonov,[5] R. St. Denis,[17] W. K. Sakumoto,[40] D. Saltzberg,[6] C. Sanchez,[32] A. Sansoni,[15] L. Santi,[47] S. Sarkar,[42] P. Savard,[46] A. Savoy-Navarro,[13] P. Schlabach,[13] E. E. Schmidt,[13] M. P. Schmidt,[52] M. Schmitt,[31] L. Scodellaro,[35] A. Scribano,[37] A. Sedov,[39] S. Seidel,[30] Y. Seiya,[48] A. Semenov,[11] F. Semeria,[3] M. D. Shapiro,[24] P. F. Shepard,[38] T. Shibayama,[48] M. Shimojima,[48] M. Shochet,[10] A. Sidoti,[35] A. Sill,[45] P. Sinervo,[46] A. J. Slaughter,[52] K. Sliwa,[49] F. D. Snider,[13] R. Snihur,[25] M. Spezziga,[45] F. Spinella,[37] M. Spiropulu,[7] L. Spiegel,[13] A. Stefanini,[37] J. Strologas,[30] D. Stuart,[7] A. Sukhanov,[14] K. Sumorok,[26] T. Suzuki,[48] R. Takashima,[19] K. Takikawa,[48] M. Tanaka,[2] M. Tecchio,[27] R. J. Tesarek,[13] P. K. Teng,[1] K. Terashi,[41] S. Tether,[26] J. Thom,[13] A. S. Thompson,[17] E. Thomson,[32] P. Tipton,[40] S. Tkaczyk,[13] D. Toback,[44] K. Tollefson,[28] D. Tonelli,[37] M. Tönnesmann,[28] H. Toyoda,[33] W. Trischuk,[46] J. Tseng,[26] D. Tsybychev,[14] N. Turini,[37] F. Ukegawa,[48] T. Unverhau,[17] T. Vaiciulis,[40] A. Varganov,[27] E. Vataga,[37] S. Vejcik III,[13] G. Velev,[13] G. Veramendi,[24] R. Vidal,[13] I. Vila,[8] R. Vilar,[8] I. Volobouev,[24]

M. von der Mey,[6] R. G. Wagner,[2] R. L. Wagner,[13] W. Wagner,[22] Z. Wan,[43] C. Wang,[12] M. J. Wang,[1] S. M. Wang,[14] B. Ward,[17] S. Waschke,[17] D. Waters,[25] T. Watts,[43] M. Weber,[24] W. C. Wester III,[13] B. Whitehouse,[49] A. B. Wicklund,[2] E. Wicklund,[13] H. H. Williams,[36] P. Wilson,[13] B. L. Winer,[32] S. Wolbers,[13] M. Wolter,[49] S. Worm,[43] X. Wu,[16] F. Würthwein,[26] U. K. Yang,[10] W. Yao,[24] G. P. Yeh,[13] K. Yi,[21] J. Yoh,[13] T. Yoshida,[33] I. Yu,[23] S. Yu,[36] J. C. Yun,[13] L. Zanello,[42] A. Zanetti,[47] F. Zetti,[24] and S. Zucchelli[3]

(CDF Collaboration)

[1]*Institute of Physics, Academia Sinica, Taipei, Taiwan 11529, Republic of China*
[2]*Argonne National Laboratory, Argonne, Illinois 60439, USA*
[3]*Istituto Nazionale di Fisica Nucleare, University of Bologna, I-40127 Bologna, Italy*
[4]*Brandeis University, Waltham, Massachusetts 02254, USA*
[5]*University of California at Davis, Davis, California 95616, USA*
[6]*University of California at Los Angeles, Los Angeles, California 90024, USA*
[7]*University of California at Santa Barbara, Santa Barbara, California 93106, USA*
[8]*Instituto de Fisica de Cantabria, CSIC-University of Cantabria, 39005 Santander, Spain*
[9]*Carnegie Mellon University, Pittsburgh, Pennsylvania 15213, USA*
[10]*Enrico Fermi Institute, University of Chicago, Chicago, Illinois 60637, USA*
[11]*Joint Institute for Nuclear Research, RU-141980 Dubna, Russia*
[12]*Duke University, Durham, North Carolina 27708, USA*
[13]*Fermi National Accelerator Laboratory, Batavia, Illinois 60510, USA*
[14]*University of Florida, Gainesville, Florida 32611, USA*
[15]*Laboratori Nazionali di Frascati, Istituto Nazionale di Fisica Nucleare, I-00044 Frascati, Italy*
[16]*University of Geneva, CH-1211 Geneva 4, Switzerland*
[17]*Glasgow University, Glasgow G12 8QQ, United Kingdom*
[18]*Harvard University, Cambridge, Massachusetts 02138, USA*
[19]*Hiroshima University, Higashi-Hiroshima 724, Japan*
[20]*University of Illinois, Urbana, Illinois 61801, USA*
[21]*The Johns Hopkins University, Baltimore, Maryland 21218, USA*
[22]*Institut für Experimentelle Kernphysik, Universität Karlsruhe, 76128 Karlsruhe, Germany*
[23]*Center for High Energy Physics: Kyungpook National University, Taegu 702-701, Korea; Seoul National University, Seoul 151-742, Korea;*
and SungKyunKwan University, Suwon 440-746, Korea
[24]*Ernest Orlando Lawrence Berkeley National Laboratory, Berkeley, California 94720, USA*
[25]*University College London, London WC1E 6BT, United Kingdom*
[26]*Massachusetts Institute of Technology, Cambridge, Massachusetts 02139, USA*
[27]*University of Michigan, Ann Arbor, Michigan 48109, USA*
[28]*Michigan State University, East Lansing, Michigan 48824, USA*
[29]*Institution for Theoretical and Experimental Physics, ITEP, Moscow 117259, Russia*
[30]*University of New Mexico, Albuquerque, New Mexico 87131, USA*
[31]*Northwestern University, Evanston, Illinois 60208, USA*
[32]*The Ohio State University, Columbus, Ohio 43210, USA*
[33]*Osaka City University, Osaka 588, Japan*
[34]*University of Oxford, Oxford OX1 3RH, United Kingdom*
[35]*Universita di Padova, Istituto Nazionale di Fisica Nucleare, Sezione di Padova, I-35131 Padova, Italy*
[36]*University of Pennsylvania, Philadelphia, Pennsylvania 19104, USA*
[37]*Istituto Nazionale di Fisica Nucleare, University and Scuola Normale Superiore of Pisa, I-56100 Pisa, Italy*
[38]*University of Pittsburgh, Pittsburgh, Pennsylvania 15260, USA*
[39]*Purdue University, West Lafayette, Indiana 47907, USA*
[40]*University of Rochester, Rochester, New York 14627, USA*
[41]*Rockefeller University, New York, New York 10021, USA*
[42]*Instituto Nazionale de Fisica Nucleare, Sezione di Roma, University di Roma I, "La Sapienza," I-00185 Roma, Italy*
[43]*Rutgers University, Piscataway, New Jersey 08855, USA*
[44]*Texas A&M University, College Station, Texas 77843, USA*
[45]*Texas Tech University, Lubbock, Texas 79409, USA*
[46]*Institute of Particle Physics, University of Toronto, Toronto M5S 1A7, Canada*
[47]*Istituto Nazionale di Fisica Nucleare, University of Trieste / Udine, Italy*
[48]*University of Tsukuba, Tsukuba, Ibaraki 305, Japan*
[49]*Tufts University, Medford, Massachusetts 02155, USA*

[50]Waseda University, Tokyo 169, Japan
[51]University of Wisconsin, Madison, Wisconsin 53706, USA
[52]Yale University, New Haven, Connecticut 06520, USA
(Received 19 April 2004; published 21 October 2004)

We present a measurement of the isolated direct photon cross section in $p\bar{p}$ collisions at $\sqrt{s} = 1.8$ TeV and $|\eta| < 0.9$ using data collected between 1994 and 1995 by the Collider Detector at Fermilab (CDF). The measurement is based on events where the photon converts into an electron-positron pair in the material of the inner detector, resulting in a two track event signature. To remove $\pi^0 \rightarrow \gamma\gamma$ and $\eta \rightarrow \gamma\gamma$ events from the data we use a new background subtraction technique which takes advantage of the tracking information available in a photon conversion event. We find that the shape of the cross section as a function of photon p_T is poorly described by next-to-leading-order QCD predictions, but agrees with previous CDF measurements.

DOI: 10.1103/PhysRevD.70.074008 PACS numbers: 13.85.Qk, 12.38.Qk

I. INTRODUCTION

The CDF Collaboration recently published a measurement of the direct photon cross section [1]. This analysis found that the shape of the cross section as a function of p_T is poorly described by next-to-leading-order (NLO) QCD calculations [2], and that the discrepancy persists at $\sqrt{s} = 1800$ GeV and 630 GeV. A similar conclusion has been reached by the D0 collaboration [3,4], and by other hadron-hadron experiments [5]. CDF and D0 both observe a cross section excess at low p_T, while at high p_T CDF finds a deficit where D0 agrees with the theoretical prediction. The difference between the CDF and D0 measurements at high p_T is within the combined systematic uncertainties of the two experiments.

Photon measurements in hadron collisions are complicated by the large number of $\pi^0 \rightarrow \gamma\gamma$ and $\eta \rightarrow \gamma\gamma$ events produced in these experiments. These backgrounds are traditionally suppressed by requiring that the photon be isolated from other energy in the calorimeter, but this requirement also eliminates some of the direct photon signal. Special calculations which take the isolation requirement into account have been developed in order to compare these measurements to NLO QCD [2].

To remove the remaining meson events from the data sample, experimentalists have relied upon understanding the shape and development of electromagnetic (EM) showers in the calorimeter . At CDF two techniques are used: a shower transverse profile method, and a preshower method [1]. The data sets are based on photon triggers, where a high E_T EM shower is found in the central calorimeter with no associated charged tracks.

In this article we report on a new measurement of the direct photon cross section at CDF based on events where the photon converts to an e^+e^- pair in the detector material prior to passing through the central tracking chamber. The EM showers in these events have tracks associated with them, and so are explicitly rejected by conventional photon measurements. Furthermore, the addition of tracking information to the event makes possible a new background subtraction technique which is systematically independent from the standard calorimeter methods.

The primary motivation for studying the direct photon cross section is the potential to extract information about the parton distribution function (PDF) of the gluon inside the proton, due to the large contribution of $gq \rightarrow \gamma q$ diagrams to the process [6]. This program has been frustrated by differences between the measurements and calculations which are difficult to explain by altering the gluon PDF alone [7–9]. The direct photon cross section measurement with conversions therefore serves as a cross check of conventional photon techniques, as well as a demonstration of a new method for future high p_T photon studies.

II. DETECTOR AND DATA SETS

The data was collected at the Fermilab TeVatron collider between 1994 and 1995 (Run 1b) with a center-of-mass energy of 1.8 TeV. A detailed description of CDF in Run 1 may be found elsewhere [10]. Here we briefly describe those detector components critical for the conversion measurement. The central tracking system consists of a silicon vertex detector (SVX), a vertex TPC (VTX), and a large central tracking chamber (CTC). These detectors are located inside a 1.4 T solenoidal magnet. The transverse momenta of charged particles in the tracking system are measured primarily by the CTC, which has a momentum resolution of $\sigma(p_T)/p_T^2 = 0.002\ \mathrm{GeV}^{-1}$. Outside the tracking system are the CDF calorimeters, which are subdivided in η [11,15] and ϕ into projective towers which point to the nominal $p\bar{p}$ interaction point at the center of the detector. The central region ($|\eta| < 1.1$) is instrumented with the central electromagnetic (CEM), central hadronic (CHA), and wall hadronic (WHA) calorimeters. EM showers in the CEM generally deposit their energy in two or three towers in η, and these towers are referred to as a CEM cluster. The energy resolution of the CEM is

$$\frac{\sigma(E)}{E} = \sqrt{\left(\frac{13.5\%}{\sqrt{E\sin\theta}}\right)^2 + (1.6\%)^2}$$

where θ is the polar angle of the shower measured with respect to the proton beam direction. The CEM is equipped with a layer of crossed wire and strip gas chambers (CES) located at a depth of six radiation lengths (the typical shower maximum) to measure the transverse shape of the shower. A second layer of wire chambers, known as the CPR, is located between the solenoid and the CEM. The CPR is used as a preshower detector in conventional photon measurements, with the 1.1 X_0 radiation lengths of the solenoid acting as the converting material.

We use a three level trigger system to collect the two data sets used in the photon cross section measurement with conversions. The first data sample, known as the 8 GeV electron data, requires a cluster in the CEM of at least 8 GeV at Level 1. Level 2 requires an associated track found by the fast hardware track finder (CFT) with $p_T >$ 7.5 GeV, and an associated CES cluster found by a hardware cluster finder (XCES). This trigger applies several electron identification requirements at Level 3, including requirements on the transverse shape of the shower seen in the CES, the geometric matching between the shower and the track, the lateral sharing of the shower energy over the several CEM towers, and the electromagnetic fraction of the shower. The integrated luminosity of this data set is 73.6 pb^{-1}.

The second data sample, known as the 23 GeV photon data, requires an 8 GeV CEM cluster at Level 1, but at Level 2 this requirement is increased to 23 GeV. The Level 2 trigger also applies an isolation requirement to the CEM cluster by requiring that the neighboring calorimeter towers have $E_T < 4$ GeV. The 23 GeV photon trigger does not require that a track be found by the CFT, and it does not apply any electron identification requirements, although at least one CES cluster must be found with more than 0.5 GeV of energy at Level 3. Note that this trigger was designed to collect nonconversion photons (hence its name), but since it does not veto photon candidates which have associated tracks, we can use it to search for conversion events as well. The integrated luminosity is 83.7 pb^{-1}.

Inner detector photon conversions are characterized by two opposite sign CTC tracks which pass near each other in the material of the beampipe, SVX, VTX, or inner cylinder of the CTC . Two conversion identification requirements are applied to the raw CTC tracks. The first requires that the absolute value of the difference between the track cotθs be less than 0.05. The second requires that the absolute value of the distance between the tracks in the transverse plane at the radial location where they are parallel be less than 0.3 cm. The distributions for these two quantities are shown in Fig. 1. At least one of these tracks is required to point at a CEM cluster, and the softer track is required to have $p_T > 0.4$ GeV.

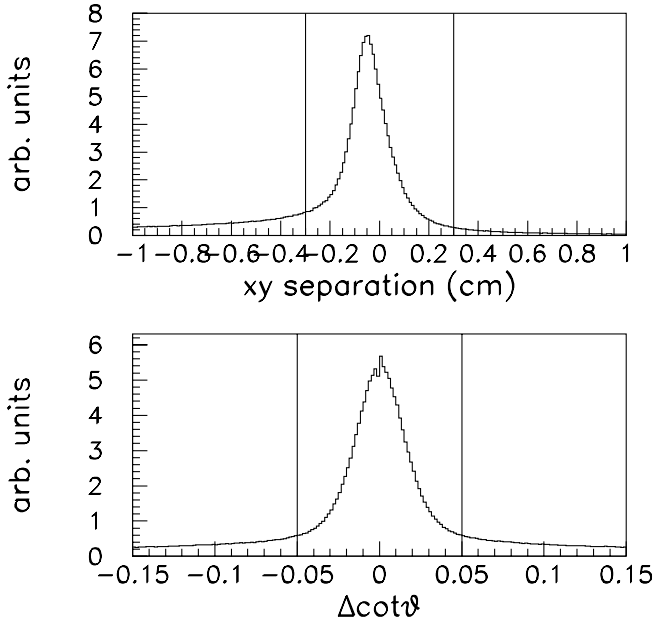

FIG. 1. The two conversion identification requirements. Events between the vertical lines are accepted as conversion candidates, while events in the tails are dominated by fakes. No other selection requirements have been applied to the data in these plots. Top: the spatial separation in the transverse plane between the tracks at the radial location where they are parallel. If the tracks cross each other they are considered to have negative separation. Bottom: the difference in the track cotθs.

Track pairs satisfying these requirements are fitted to a conversion vertex. The fit requires that the tracks meet at a point in space where they are parallel, which improves the spatial and momentum resolutions of the reconstructed photon candidate. In addition, the vertex fit partially corrects for a p_T bias present in the raw conversion tracks. This bias occurs when the spatial separation of the conversion tracks in the inner CTC superlayers is less than the two track resolution of the device. The final requirement of the conversion selection is that the fitted conversion radius is required to be between 2 and 30 cm. The radius of conversion distribution of the 8 GeV electron data is shown in Fig. 2.

Conversion candidate events at CDF divide naturally into two sets based on their detector topology. In 1-tower conversions both tracks point to the same CEM tower, and in 2-tower conversions the tracks point to separate towers. 1-tower conversions have the potential to confuse the electron identification requirements applied by the 8 GeV electron trigger at Level 3, due to the presence of two EM showers in the same CES chamber. Therefore in the 8 GeV electron data we require that the conversion be 2-tower. Conversely, in the 23 GeV photon data we require that the conversion be 1-tower, in order to insure that the two data sets have no events in common.

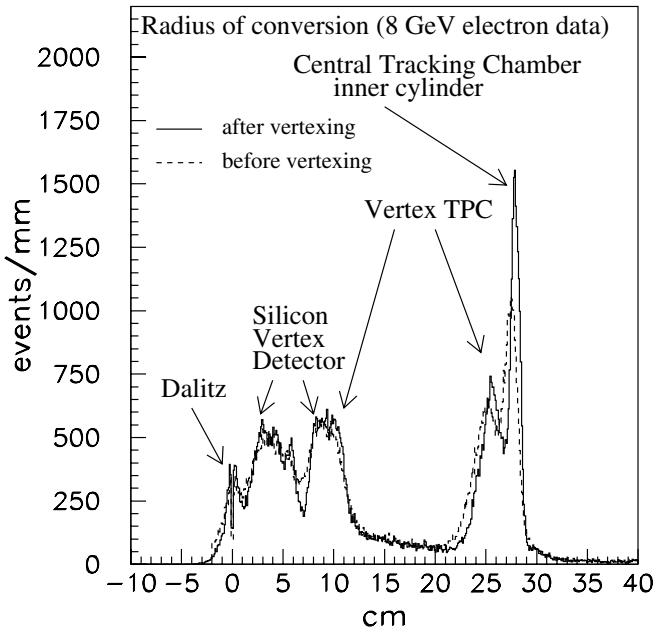

FIG. 2. Vertexed and unvertexed radius of conversion distribution in 8 GeV electron data. The peak at $r = 0$ labeled 'Dalitz' is due to $\pi^0 \to e^+e^-\gamma$ decays and $\gamma^* \to e^+e^-$ events. The 2 cm $< r <$ 30 cm data selection requirement has been released in this plot.

In a 1-tower event, the CEM cluster measures the summed E_T of both tracks. In a 2-tower event, however, the softer track is outside the high E_T cluster formed by the first track, and its own E_T usually falls below the clustering threshold of the CEM reconstruction algorithm. In this case, only the higher E_T cluster is found, but the p_T of both tracks is measured by the CTC. When dividing the conversion events into p_T bins, we use the summed E_T measurement for 1-tower events, while for 2-tower events we use the E_T measurement of the higher energy track plus the p_T measurement of the lower energy track.

The offline data reduction proceeds as follows. For the 8 GeV electron data we require a 2-tower conversion at $|\eta| < 0.9$ and $|z_0| < 60$ cm, where z_0 is the position of the primary event vertex along the beamline measured from the center of the detector. The conversion must be associated with a fiducial CEM cluster, and we reapply the electron identification requirements imposed by the Level 3 trigger. The reconstructed CEM cluster must have $E_T >$ 8.0 GeV, and at least one of the conversion tracks must have $p_T > 6.0$ GeV. To suppress the contribution of π^0 and η events we make two isolation requirements. The first requires that the amount of energy found in a cone of radius $R = \sqrt{(\Delta\eta)^2 + (\Delta\phi)^2}$ less than 0.4 centered on the highest E_T shower be less than 1 GeV, excluding the energy in the CEM cluster itself. The second requires that no extraneous tracks with $p_T > 0.4$ GeV point to the CEM cluster. Finally we require that the missing energy ($\not\!\!E_T$) in this data set be less than 25 GeV in order to suppress a background due to $W \to e\nu$ events.

For the 23 GeV photon data we require a 1-tower conversion at $|\eta| < 0.9$ and $|z_0| < 60$ cm with a fiducial CEM cluster and the same isolation requirements. The CEM cluster must have $E_T > 28$ GeV and the conversion must have at least one track with $p_T > 8.0$ GeV. This data set has no electron identification requirements, and no $\not\!\!E_T$ requirement.

There is one complication to the cone 0.4 isolation requirement in the case of a 2-tower conversion. If the soft conversion track lands outside the CEM cluster, but within the 0.4 cone, then the cone energy sum is artificially enhanced by the energy of this track. To remove this energy the tower hit by the soft track and its closest neighbor in η are excluded from the cone energy sum. In this case the area of the cone is slightly reduced, and to account for this the energy requirement is reduced from 1.0 GeV to 0.87 GeV. This occurs in about 2/3 of all 2-tower events.

III. BACKGROUND SUBTRACTION

A. π^0 and η backgrounds

Most $\pi^0 \to \gamma\gamma$ and $\eta \to \gamma\gamma$ events are rejected by the isolation requirements. Those that remain are statistically subtracted from the data by a new technique based on E/p. E/p is the ratio of the E_T measured in the CEM and the p_T measured by the CTC. For a 1-tower conversion the E_T is the two track summed energy measured by the CEM, and the p_T is the sum of the two vertexed track momenta. For a 2-tower conversion, the CEM cluster measures only the E_T of the higher energy track, and in this case the E/p ratio includes only the E_T and vertexed p_T of that track.

Under this definition, the E/p distribution for a direct photon conversion should be a narrow peak centered on 1.0 whose width is determined by the CTC and CEM resolutions. In a π^0 or η event, however, the second unconverted photon usually showers in the same CEM cluster as the high E_T conversion electron. Therefore in a meson event the E_T measures the π^0 energy, and the p_T measures the energy of one of the decay photons. Since two-body decay kinematics are understood, the shape of the meson E/p distribution is relatively easy to calculate with a Monte Carlo simulation.

To predict the signal E/p distribution we generate direct photon events using PYTHIA version 6.115 [11]. The prompt photon is tracked through a material map of the CDF inner detector where it is allowed to convert into an electron-positron pair. The two tracks pass through the remaining material, where they are allowed to undergo bremsstrahlung, and through the tracking chamber and calorimeter. To simulate the p_T and E_T measurements the true track parameters are smeared by the known resolutions of the CTC and CEM.

We find that for the purpose of predicting the meson E/p distribution, it is adequate to simulate single mesons, rather that complete events, because the mesons in the data are highly isolated. The generated mesons decay to two photons which are tracked through the detector in the same manner as the PYTHIA direct photons. The two meson samples are combined using a η/π^0 production ratio of 0.69 ± 0.08, which we measured in the data using a sample of double conversion ($\pi^0/\eta \to \gamma\gamma \to e^+e^-e^+e^-$) events, as shown in Fig. 3. Fortunately, the E/p distributions of π^0 and η are very similar (due to similar decay kinematics), so the production ratio used in the Monte Carlo has little effect on their combined E/p shape. We also use the double conversion events to measure the meson p_T spectrum to be used in the Monte Carlo. We find that a power law with an exponent of negative six gives a good description of the data.

We extract the number of signal candidates in each p_T bin by performing a χ^2 fit of the E/p distributions observed in the data to the Monte Carlo signal and background templates. In the fit only the normalizations of the signal and background are allowed to float. Examples of two fits are shown in Fig. 4.

As seen in Fig. 4, the narrow signal peak is quite distinct from the broad background distribution, and there is good agreement between data and Monte Carlo in the high E/p tail region. This indicates that the Monte Carlo prediction of the E/p shape of the background is robust. Most of the fits return a confidence level greater than 5%, with a flat distribution up to 100%. In some p_T bins, however, the narrow signal peak is shifted slightly with respect to the Monte Carlo prediction, and these fits have a large χ^2. This effect is due to a p_T bias associated with

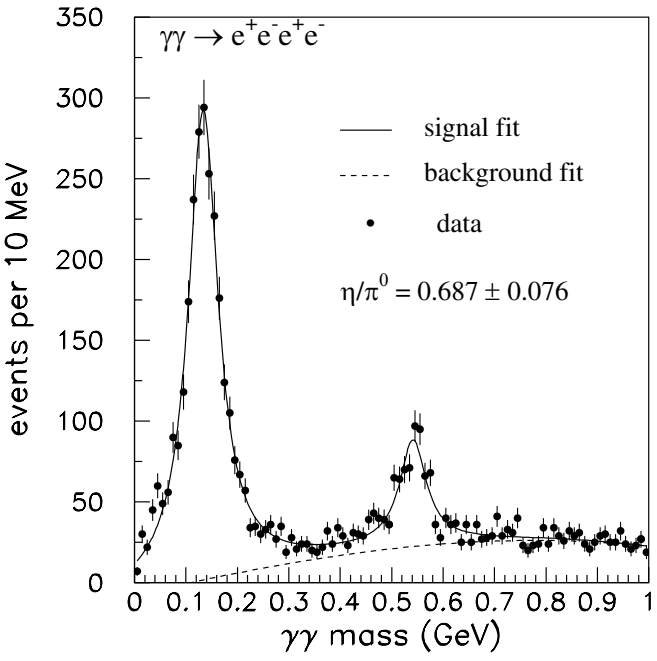

FIG. 3. The diphoton mass spectrum of double conversion events in the data. The data is fit to two Lorentzians plus a third order polynomial. The polynomial is shown as the dotted line. The π^0 and η peaks are visible at 0.135 GeV and 0.547 GeV, respectively. The ratio of the areas of the two peaks, along with the Monte Carlo prediction for the ratio of acceptances, gives an η/π^0 production ratio of 0.687 ± 0.076.

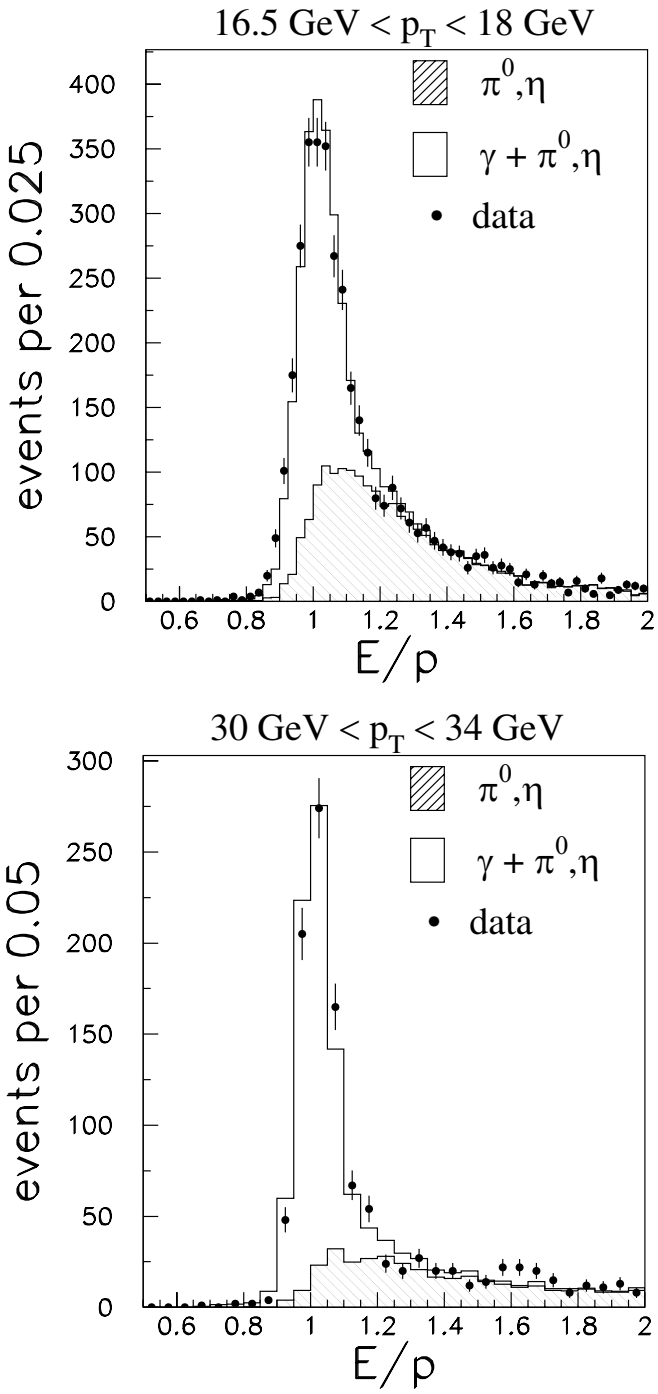

FIG. 4. An example of the E/p background subtraction fit in two p_T bins. The 16.5 to 18 GeV bin is from the 8 GeV electron (2-tower) data, and the 30 to 34 GeV bin is from the 23 GeV photon (1-tower) data.

conversion tracking which occurs when the spatial separation of the two tracks in the inner layers of the CTC is below the hit resolution. A hit level simulation of the tracking system reproduces this effect, but it is not simulated by our fast Monte Carlo, so the templates do not reproduce this. Studies show that the E/p shift is no larger than 1% in the 8 GeV electron data, and 2% in the 23 GeV photon data [12].

To determine a systematic uncertainty on the background subtraction due to this effect, we multiply the E/p of each event in the 8 GeV electron data by scale factors of 1.01 and 0.99. We then perform the χ^2 fit again, and we take the change in the number of signal candidates as a systematic uncertainty. Similarly we use scale factors of 1.02 and 0.98 in the 23 GeV data to determine the uncertainty. For the 8 GeV electron data this error is $+12/-10\%$ at 10 GeV and decreases to less than $\pm 5\%$ above 20 GeV, while the error is less than $\pm 5\%$ for the 23 GeV photon data.

B. Other backgrounds

We consider two other potential sources of background. The first is fake conversions, where two random tracks satisfy the conversion identification requirements. In this case the soft conversion track is likely to be a hadron. A study of the E/p of the soft conversion tracks finds no evidence for hadronic contamination, so we neglect this background.

A second source of background is due to high p_T prompt electrons, such as those produced in $W \rightarrow e\nu$ events. These electrons often have a co-linear bremsstrahlung photon, and this photon may convert in the detector material and produce one or two soft tracks. The soft tracks can form a high p_T conversion candidate when combined with the prompt electron. This background is the motivation for the $\not\!\!E_T$ requirement applied to the 8 GeV electron data, which would otherwise have significant $W \rightarrow e\nu$ contamination above 25 GeV. In the 23 GeV photon data this background is less significant because these events are unlikely to satisfy the 1-tower topology.

To account for remaining prompt electron backgrounds in both data sets, including any remaining W electrons, we have searched for hits in the SVX and VTX detectors in events where the conversion occurs outside these detectors. These studies have indicated that in the 8 GeV electron data there is no significant prompt electron contamination below 25 GeV, and above 25 GeV we adopt a one sided 10% systematic uncertainty. In the 23 GeV photon data we adopt a one sided 3% systematic uncertainty in all p_T bins.

IV. ACCEPTANCE AND EFFICIENCY

The acceptance is evaluated with the PYTHIA direct photon Monte Carlo, and includes the fiducial requirements, the 1-tower and 2-tower topological requirements, and the E_T and p_T requirements on the CEM clusters and tracks. For the 2-tower data (8 GeV electron trigger), the acceptance decreases from 33% at 10 GeV to 6.5% at 65 GeV, due to the fact that the 2-tower geometry is kinematically disfavored at high p_T. The 1-tower data (23 GeV photon trigger), on the other hand, is favored at high p_T, and its acceptance increases from 35% at 30 GeV to 43% at 65 GeV.

The efficiency of the remaining selection requirements are measured in the data with a variety of complementary data sets [12]. To measure the conversion identification efficiency, we relax the requirement on the difference in track $\cot\theta$ from 0.05 to 0.15 and the requirement on the separation in the transverse plane from 0.3 cm to 1.0 cm. In this loose sample the conversions in the material of the CTC inner cylinder still dominate the fake conversions at that large radius. Since fake conversions have a smooth radius-of-conversion distribution, we remove them with a sideband subtraction, and the efficiency is the ratio of the number of real conversions found with the standard requirements to the number found with the relaxed requirements. We find an efficiency of $97.4 \pm 2.0\%$, where the uncertainty is determined by variations seen when dividing the data into p_T bins .

The efficiency of the event z_0 requirement is measured to be $93.7 \pm 1.1\%$ in minimum bias data. The 8 GeV electron trigger efficiency is measured with a prescaled 5 GeV electron trigger and an inclusive muon data set, and has an asymptotic efficiency of $91.4 \pm 0.9\%$. The 23 GeV photon trigger efficiency is measured with prescaled 10 GeV and 23 GeV photon triggers, and has an efficiency of $91.4 \pm 4.3\%$ [13]. The electron identification efficiency is measured with the nontrigger electron in $Z \rightarrow e^+e^-$ data, and is found to be $84.3 \pm 3.0\%$.

The CTC tracking efficiency is measured by embedding Monte Carlo tracks into the hit data of real events, and then measuring the efficiency with which the tracking reconstruction code finds the new track in the event. We find that the tracking efficiency has a plateau value of $96 \pm 2\%$ per track above 400 MeV.

The isolation requirement efficiency is measured by choosing random locations in the calorimeter in minimum bias data and adding up the energy found within a cone radius of 0.4. This procedure assumes that the energy in the calorimeter due to the underlying event and multiple $p\bar{p}$ interactions is similar to the energy found in minimum bias data. This assumption has been checked by comparing with the energy found in the calorimeter in 70 GeV photon data. In that study we measured the average energy found in the calorimeter 90° away from the photon in azimuth. We found that the photon data had slightly more energy than the minimum bias data, and we take the difference as a systematic error on the isolation cut efficiency. A second study with lower energy photon

TABLE I. Summary of signal efficiencies. The asterisks indicate to which data set each efficiency applies.

source	8 GeV electron	23 GeV photon	efficiency
z_0	*	*	0.937 ± 0.011
Conversion ID	*	*	0.974 ± 0.020
Level 1 trigger	*	*	1.0
Level 2 trigger (8 GeV)	*		$91.4 \pm 0.9\%$ above 16 GeV
Level 2 trigger (23 GeV)		*	0.914 ± 0.043
Level 3 electron ID	*		0.849 ± 0.030
Tracking (CTC)	*	*	0.96 ± 0.02 per track
Isolation	*	*	0.859 ± 0.004
No extra tracks	*	*	0.896 ± 0.005
$\not\!\!E_T$	*		1.0 below 20 GeV, 0.89 at 65 GeV

data gave similar results, and we concluded that the underlying event energy does not depend on the p_T of the photon. However, the underlying event energy does correlate well with the number of primary event vertices reconstructed by the VTX. Therefore we measure the isolation cut efficiency as a function of the number of interactions, and then convolute the measured values with the number-of-vertices distribution observed in the conversion data. The efficiency is found to be $85.9 \pm 0.4\%$.

The no-extra-track requirement efficiency is evaluated with electrons in $Z \rightarrow e^+e^-$ data, and is found to be $89.6 \pm 0.5\%$. The missing energy efficiency is evaluated with unisolated conversion candidates. These events are predominantly di-jet events where the true $\not\!\!E_T$ is zero, so the measured $\not\!\!E_T$ is due to the calorimeter resolution. The efficiency decreases from 1.0 at 20 GeV to 89% at 65 GeV.

The efficiencies are summarized in Table I. The total acceptance times efficiency for the two data sets is plotted in Fig. 5.

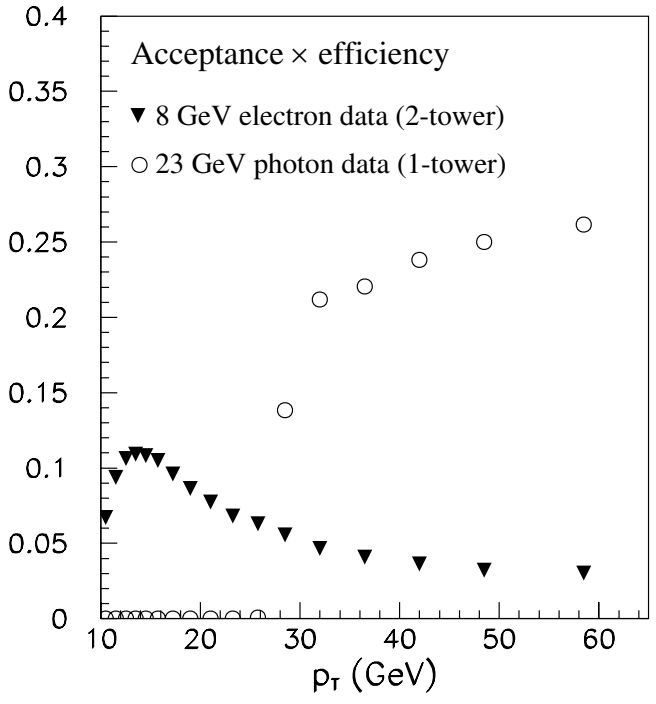

FIG. 5. The total acceptance times efficiency for both conversion data sets. The decrease in the acceptance at high p_T for the 8 GeV electron data set is due to the 2-tower requirement, which becomes geometrically disfavored. The total conversion probability is not included here.

V. TOTAL CONVERSION PROBABILITY

The final element of the photon cross section measurement with conversions is the total probability that the photon converts in the CDF inner detector. The conversion probability has been evaluated in several ways. The standard technique relies on a material map measured in the data with an inclusive conversion data set, calibrated with an *a priori* determination of the amount of material in the CTC inner cylinder. This method gives a conversion probability of $5.17 \pm 0.28\%$, and we refer to this result as the standard material scale. Other material measurements based on the hard bremsstrahlung rate in $W \rightarrow e\nu$ and $J/\psi \rightarrow e^+e^-$ events give results in agreement with this number [14].

A second technique compares the number of π^0 Dalitz decays ($\pi^0 \rightarrow e^+e^-\gamma$) to the number-of $\pi^0 \rightarrow \gamma\gamma$ decays. In some Dalitz events the on shell photon subsequently converts in the inner detector material. Then the event has a four track topology, with the invariant mass being the π^0 mass. Similarly, in some $\gamma\gamma$ events both photons convert in the detector material, giving the same four track signature. In the four track event sample, the Dalitz events can be separated from the $\gamma\gamma$ events because two of the Dalitz electrons are prompt. Since the four track Dalitz events undergo one conversion in the detector material, while the four track $\gamma\gamma$ events undergo two conversions, the Dalitz-to-$\gamma\gamma$ ratio gives the conversion probability, after accounting for the branching ratios of the two decays. This method gives a conversion probability of $8.02 \pm 0.73(stat) \pm 0.73(sys)\%$, which is significantly higher than the standard result quoted above.

Several other data sets also give evidence for a larger conversion probability. At CDF the reconstructed mass of di-muon resonances such as the J/ψ, $\psi(2s)$, $\Upsilon(1s)$,$(2s)$, and $(3s)$ depend on the amount of material in the inner detector due to muon dE/dx energy losses. We correct the muon momenta for the expected energy loss by assuming the standard material scale. However, after the correction the reconstructed masses are less than the PDG masses for all five resonances. For the J/ψ the mass shift is more than 20 times larger than the statistical error, while for the $\Upsilon(3s)$ the shift is only 1.2 times the statistical error. The dominant systematic uncertainty is due to the fact that the reconstructed J/ψ mass depends on the amount of material the muons pass through [14]. After adopting a systematic uncertainty to account for this, the measured value of the J/ψ mass agrees with the PDG value within errors. These effects do not prove that the standard material scale is too small, but they are consistent with that hypothesis.

There is also some evidence from W electrons for a larger material scale. In Run 1b the peak of the E/p distribution in W electrons in the data is shifted to the right with respect to the Monte Carlo simulation when assuming the standard material scale. Although this effect is not adequately understood, the Monte Carlo E/p peak can be made to agree with the data by increasing the material [14].

In summary, the evidence concerning the total conversion probability is ambiguous. Rather than choose between two conflicting results, we adopt the approach of choosing a central value and systematic uncertainty which encompasses all possibilities. This value is $6.60 \pm 1.43\%$. We make one adjustment to the conversion probability to account for the effective loss of material due to the requirement on the radial location of the conversion ($r_{cnv} > 2.0$ cm). The final value of the effective conversion probability is $6.40 \pm 1.43\%$. The uncertainty on the conversion probability dominates all other errors on the photon cross section. However, while the conversion probability affects the overall normalization of the cross section, it does not affect the shape of the cross section as a function of p_T. This is assured by the fact that the pair-production cross section does not vary significantly over the p_T range considered here.

VI. SYSTEMATIC UNCERTAINTIES

In this section we briefly summarize the systematic uncertainties on the photon cross section measurement with conversions. (A detailed discussion is given in Ref. [12].) In Section III we discussed the systematic uncertainties we adopt to account for shortcomings in the Monte Carlo E/p model, and backgrounds due to prompt electrons. Both of these uncertainties depend on p_T.

For the 8 GeV electron data the remaining p_T dependent systematic uncertainties are as follows. We take a systematic uncertainty to account for a possible time dependence on the trigger efficiency. This uncertainty is determined by counting the fraction of events in our final sample which occur before the midpoint of Run 1b. This fraction is 53.6%, and depends on p_T. We take 3.6% as the uncertainty. Secondly, the conversion identification efficiency varies by 2.0% when dividing the data into p_T bins, and we take this as a systematic uncertainty.

We also adopt the following p_T independent systematic uncertainties. The cross section uncertainty due the total conversion probability is $+27/-17\%$. The CEM energy scale uncertainty results in a cross section error of 3.0%. The integrated luminosity is measured to 4.1%, and the asymptotic trigger efficiency is known to 1.4%. There are also uncertainties due to the tracking efficiency (2.0%), the electron identification efficiency (3.5%), and the z_0 requirement efficiency (1.2%).

The systematic uncertainties on the 23 GeV photon data sample are similar, except there is no trigger time dependence, no electron identification uncertainty, and the asymptotic trigger efficiency is known to 4.7%.

The total p_T independent systematic uncertainty is $+28/-18\%$ for both data sets. The total p_T dependent

TABLE II. The p_T dependent systematic uncertainty for all p_T bins. The correlated systematic uncertainty is +28/-18% for both data sets.

p_T (GeV)	p_T dep. sys. err. (%)
8 GeV electron (2-tower) data:	
10–11	$+10.6/-12.8$
11–12	$+9.3/-11.6$
12–13	$+9.4/-9.3$
13–14	$+8.5/-8.6$
14–15	$+6.7/-7.3$
15–16.5	$+6.7/-6.9$
16.5–18	$+5.7/-6.0$
18–20	$+7.6/-7.8$
20–22	$+7.0/-6.1$
22–24.5	$+4.3/-5.8$
24.5–27	$+5.1/-11.9$
27–30	$+5.7/-11.3$
30–34	$+4.1/-11.1$
34–39	$+4.1/-11.0$
39–45	$+5.6/-11.5$
45-52	$+4.1/-10.8$
52-65	$+8.8/-13.3$
23 GeV photon (1-tower) data:	
30–34	$+2.3/-4.9$
34–39	$+2.8/-4.9$
39–45	$+3.9/-5.6$
45–52	$+5.0/-4.7$
52–65	$+4.7/-8.2$

TABLE III. Summary of the conversion cross section measurement in both data sets. The 8 GeV electron data has an integrated luminosity of 73.6 pb^{-1}, and the 23 GeV photon data has an integrated luminosity of 83.7 pb^{-1}. $\Delta\eta$ is 1.8, and the effective conversion probability, which is not included in the acceptance $\times$ efficiency shown here, is 6.40%. The NLO QCD theory was calculated by the authors of Reference [2], and uses the CTEQ5M parton distribution functions with all scales set to the p_T of the photon.

p_T (GeV)	$\langle p_T \rangle$ (GeV)	$\mathcal{A} \cdot \epsilon$	N_{signal}	$d\sigma/dp_T d\eta$ (pb/GeV)	stat error (%)	sys error (%)	NLO QCD (pb/GeV)
8 GeV electron (2-tower) data:							
10–11	10.5	0.067	7152	12590	2.2	+30/−22	10968
11–12	11.5	0.094	7761	9771	2.1	+29/−22	7434
12–13	12.5	0.106	6111	6773	2.2	+29/−20	5203
13–14	13.5	0.109	4320	4659	2.6	+29/−20	3743
14–15	14.5	0.108	3195	3483	2.9	+29/−20	2758
15–16.5	15.7	0.105	3059	2289	2.8	+29/−20	1963
16.5–18	17.2	0.096	1846	1509	3.5	+28/−19	1328
18–20	18.9	0.086	1391	950	4.1	+29/−20	888
20–22	20.9	0.077	863	658	5.1	+29/−19	577
22–24.5	23.2	0.068	596	413	6.0	+28/−19	369
24.5–27	25.7	0.063	344	258	7.7	+28/−22	238
27–30	28.3	0.056	272	207	8.8	+28/−21	158
30–34	31.9	0.047	136	85.9	13.5	+28/−21	94.6
34–39	36.3	0.041	101	58.5	14.4	+28/−21	49.1
39–45	41.6	0.036	63.9	34.5	18.7	+28/−22	26.2
45–52	48.1	0.032	21.7	11.4	53.3	+28/−21	13.4
52–65	57.8	0.030	16.6	5.0	33.5	+29/−23	5.7
23 GeV photon (1-tower) data:							
30–34	31.9	0.212	723	88.4	4.8	+28/−19	94.6
34–39	36.3	0.220	564	53.1	5.3	+28/−19	49.1
39–45	41.6	0.238	316	22.9	7.4	+28/−20	26.2
45–52	48.1	0.250	225	13.3	8.5	+29/−19	13.4
52–65	57.8	0.261	131	4.0	11.3	+29/−21	5.7

systematic uncertainty in each p_T bin is listed in Table II. The total systematic uncertainty is listed in Table III.

VII. CROSS SECTION MEASUREMENT

The cross section is calculated according to

$$\frac{d\sigma^2}{dp_T d\eta} = \frac{N_{\text{signal}}}{A \cdot \epsilon \cdot \Delta p_T \cdot \Delta\eta \cdot \int \mathcal{L}} \tag{1}$$

$A \cdot \epsilon$ is the acceptance times efficiency shown in Fig. 5 multiplied by the effective conversion probability of 6.40%. We measure the average cross section between $-0.9 < \eta < 0.9$, so $\Delta\eta$ is 1.8. Δp_T is the bin width, and $\int \mathcal{L}$ is the integrated luminosity of 73.6 pb^{-1} for the 8 GeV electron data and 83.7 pb^{-1} for the 23 GeV photon data.

The final result for both data sets is listed in Table III. In the p_T region where the data sets overlap (30 GeV $< p_T <$ 65 GeV) the two measurements are in good agreement with each other. This comparison is an important cross check on the acceptance and efficiency calculations of the two data sets, since they differ by up to a factor of 9.

Since the two data sets are in agreement we can combine the measurements in the region of overlap. However, the 23 GeV photon data would dominate the combined cross section (due to much smaller errors), so instead we simply adopt the 23 GeV photon data above 30 GeV. This hybrid cross section is compared to NLO QCD and the standard CDF measurement (referred to as CES-CPR) in Fig. 6. The theory curve is taken from the authors of Reference [2]. The calculation uses the CTEQ5M parton distribution functions, and the renormalization, factorization, and fragmentation scales have been set to the p_T of the photon. This calculation takes into account the suppression of the bremsstrahlung diagrams due to the isolation requirement on the photon. In the lower half of Fig. 6 the measurements are shown as (data-theory)/theory.

The CES-CPR measurement and the conversion measurement agree with each other both in shape and in normalization. The total systematic uncertainty on the conversion measurement is larger ($+30/-20\%$) than the CES-CPR measurement (18% at 10 GeV and 11% at 115 GeV) due to the large uncertainty on the total conversion probability. Nevertheless, for both measurements the total systematic uncertainties are primarily p_T inde-

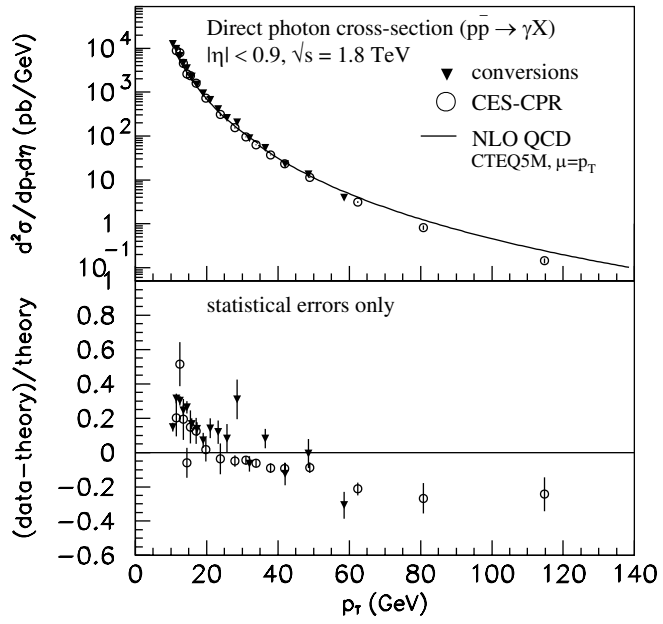

FIG. 6. The isolated direct photon cross section. The result of the conversion technique is compared with CES-CPR and theory. For the conversion measurement the 8 GeV electron data is shown below 30 GeV, and the 23 GeV photon data above. The theory curve is from the authors of Reference [2], and uses the CTEQ5M parton distribution functions with the all scales set to the p_T of the photon. Only the statistical error bars are shown here.

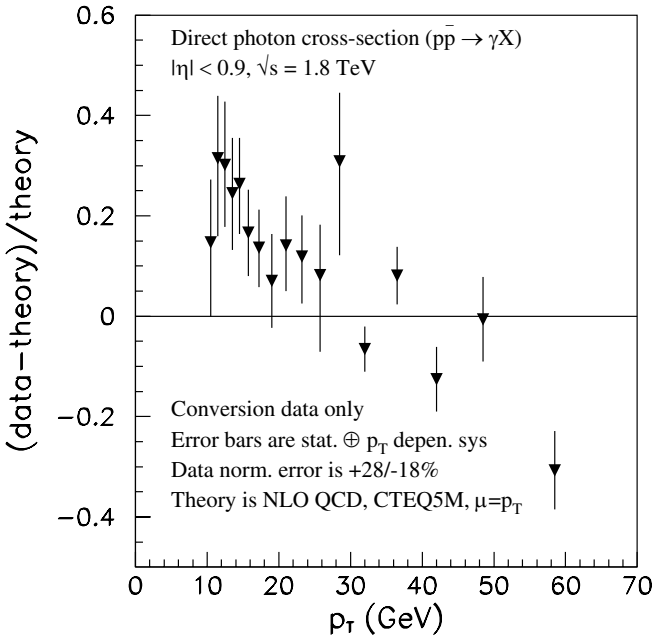

FIG. 7. The isolated photon cross section from conversions compared to NLO QCD. The error bars shown here are the combined statistical and p_T dependent systematics, in order to compare the shape of the measured cross section to theory.

pendent, so that both techniques give a much more precise measurement of the shape of the cross section as a function of p_T. The agreement of the conversion and CES-CPR measurements on the shape is remarkable, since the two techniques have little in common with each other. They use independent data samples, independent background subtraction techniques, and have different acceptances, efficiencies, and systematic uncertainties.

Figure 7 shows the conversion measurement alone as (data-theory)/theory. To compare the shape of the data to the calculation, the uncertainty bars in this plot are the combined statistical and p_T dependent systematic uncertainties. The data show a steeper slope than the calculation which is unexplained by the systematic uncertainties of the measurement. Other analyses have concluded that this type of shape difference is difficult to resolve simply by changing the renormalization, fragmentation, and factorization scales of the calculation, or the set of parton distribution functions [1]. Since two independent experimental techniques are in agreement on the shape, this is further evidence that refinements to the calculation are needed before these measurements can provide useful constraints on the gluon distribution of the proton.

ACKNOWLEDGMENTS

We would like to thank Werner Vogelsang for providing the theoretical calculations used in this paper. We also thank the Fermilab staff and the technical staffs of the participating institutions for their vital contributions. This work was supported by the U.S. Department of Energy and National Science Foundation; the Italian Istituto Nazionale di Fisica Nucleare; the Ministry of Education, Culture, Sports, Science and Technology of Japan; the Natural Sciences and Engineering Research Council of Canada; the National Science Council of the Republic of China; the Swiss National Science Foundation; the A. P. Sloan Foundation; the Bundesministerium fuer Bildung und Forschung, Germany; the Korean Science and Engineering Foundation and the Korean Research Foundation; the Particle Physics and Astronomy Research Council and the Royal Society, UK; the Russian Foundation for Basic Research; the Comision Interministerial de Ciencia y Tecnologia, Spain; work supported in part by the European Community's Human Potential Programme under Contract No. HPRN-CT-20002, Probe for New Physics; and this work was supported by Research Fund of Istanbul University Project No. 1755/21122001.

[1] CDF Collaboration, D. Acosta *et al.*, Phys. Rev. D **65**, 112003 (2002).
[2] M. Gluck, L. E. Gordon, E. Reya, and W. Vogelsang, Phys. Rev. Lett. **73**, 388 (1994).
[3] D0 Collaboration, B. Abbott *et al.*, Phys. Rev. Lett. **84**, 2786 (2000).
[4] D0 Collaboration, V. M. Abazov *et al.*, Phys. Rev. Lett. **87**, 251805 (2001).
[5] Fermilab E706 Collaboration, L. Apanasevich *et al.*, Phys. Rev. Lett. **81**, 2642 (1998).
[6] W. Vogelsang and A. Vogt, Nucl. Phys. B **453**, 334 (1995).
[7] J. Huston *et al.*, Phys. Rev. D **51**, 6139 (1995).
[8] J. Huston *et al.*, Phys. Rev. D **58**, 114034 (1998).
[9] L. Apanasevich *et al.*, Phys. Rev. D **59**, 074007 (1999).
[10] CDF Collaboration, F. Abe *et al.*, Nucl. Instrum. Methods Phys. Res., Sect. A **271**, 387 (1988).
[11] T. Sjostrand *et al.*, Comput. Phys. Commun. **135**, 238 (2001).
[12] C. Hall, Ph.D. thesis, Harvard University, 2002, available at http://www-cdf.fnal.gov/grads/thesis.html.
[13] D. Partos, Ph.D. thesis, Brandeis University, 2001, available at http://www-cdf.fnal.gov/grads/thesis.html.
[14] CDF Collaboration, T. Affolder *et al.*, Phys. Rev. D **64**, 052001 (2001).
[15] Pseudorapidity (η) is defined by $\eta = -\ln\tan(\theta/2)$, where θ is the polar angle measured from the beamline.